# A QCM-D SENSING STRATEGY FOR INVESTIGATING THE REAL-TIME EFFECTS OF OXIDATIVE STRESS ON THE VISCOELASTIC PROPERTIES OF PRE-OSTEOBLAST CELLS

Saadia Shoaib[1] and Maryam Tabrizian[1,2*]

[1]Department of Biomedical Engineering, Faculty of Medicine, [2]Faculty of Dentistry, McGill University, Montreal, Canada

## ABSTRACT

Oxidative stress results from an imbalance in the cellular redox state which can cause damage to the cell cytoskeleton and morphology, thereby affecting cell viscoelasticity. In this study, we introduce a quartz crystal microbalance with dissipation (QCM-D) sensing strategy that enables the real-time assessment of the changes in the viscoelastic properties of an MC3T3 cell monolayer in response to oxidative stress. This was successfully achieved by tracking the changes in energy dissipation ($\Delta D$-response) caused by the interaction of $H_2O_2$ with the cell monolayer adhered to a poly-D-lysine-coated polystyrene quartz sensor. While a return to baseline values of the $\Delta D$-response was obtained at 325 min (recovery point) after the incubation of cells with 25 μM $H_2O_2$, higher concentrations (50 μM-10 mM) exhibited no recovery. We successfully validated using scanning electron, atomic force and fluorescence microscopy that at the recovery point the cell morphology recovered from 25 μM $H_2O_2$ exposure, whereas, higher concentrations (50 μM-10 mM) resulted in the shrinkage of the cytoskeleton, alteration in cell morphology, and decrease in cell density due to apoptosis/necrosis, supported by a cell viability assay. Finally, total antioxidant capacity assay (TAC) confirmed that while cells' metabolic state recovered from 25 μM $H_2O_2$ treatment, higher $H_2O_2$ concentrations led to decline in TAC. Altogether, these results showed that the viscoelastic properties of cells can be used to

investigate cell recovery from oxidative stress, which may allow us to distinguish oxidative eustress from distress. Overall, we have demonstrated that QCM-D is a viable tool for measuring the effects of oxidative stress on the viscoelastic properties of MC3T3 cells.

***KEYWORDS:*** *Oxidative stress, hydrogen peroxide, viscoelastic properties, cell morphology, cell recovery, Quartz Crystal Microbalance with Dissipation*

## 1. INTRODUCTION

Oxidative stress is defined as the imbalance between the production of reactive oxygen species (ROS) and antioxidant capacity which leads to cellular damage[1]. In addition to contributing to cellular metabolic processes, ROS triggers the activation of cellular defense mechanisms which up-regulates the production of antioxidants[1]–[10]**.** Antioxidants are responsible for the removal or conversion of ROS to less reactive products. However, if the concentration of ROS exceeds the capacity of the defense mechanism, it can lead to ROS-induced oxidative damages. Previous studies have linked ROS-induced oxidative damages with the pathogenesis of numerous diseases such as neurological diseases, cardiovascular diseases, kidney diseases, cancer, age-related diseases and bone diseases[5], [11], [12]. This makes oxidative stress research of particular importance to the medical community.

ROS, such as hydrogen peroxide ($H_2O_2$) has gained increasing attention in the scientific community since it is generated as a redox metabolite in response to oxidative stress in mammalian cells. It has been recognized as an essential compound participating in normal cellular metabolism which plays a major role in various physiological pathways[1]–[5]. However, excess concentrations of $H_2O_2$ can be harmful to biomolecules of cells resulting in oxidative damage[10], [13]–[21]. For example, previous studies have shown that $H_2O_2$ caused morphological alteration in mammalian cells and consequently, led to $H_2O_2$-induced cell cycle

arrest or cell death via apoptotic or necrotic pathways[13]–[15], [22], [23]. Additionally, studies on bone marrow stromal cells and calvarial osteoblasts have demonstrated that $H_2O_2$ concentration as low as 0.1 mM inhibited expression of osteoblastic differentiation markers, while a higher concentration of $H_2O_2$ (1 mM) induced cell death[24]. These damages are most prominent during the aging process because of the poor functioning of mitochondria leading to an unrelenting cycle of ROS production[2], [25].

Cells activate a variety of complex signaling pathways in order to respond to the chemical perturbations caused by different types of exogenous stimuli, including $H_2O_2$. The underlying signaling mechanisms and associated proteins work closely with the cytoskeleton to perform basic cell functions such as growth, motility, apoptosis, differentiation, repair, and degradation. As a result, when cells are overexposed to oxidizing agents, it leads to changes in cellular redox potential and morphology which in turn affects the viscoelastic properties of cells[1], [26]–[29]. The importance of viscoelastic properties of cells in the context of cellular function and its relationship to disease pathogenesis is gaining increasing attention in the scientific community[27], [30], [31]. The interior of the cell consists of a high-water content, and highly complex and dynamic protein network. This allows the cells to store and dissipate energy depending on the rate of internal or external perturbations, which translates into the changes in the viscoelastic behavior of cells[32]. When cells are subjected to different biological and chemical perturbations, the cellular architecture can be altered due to changes in the cytoskeletal structure [30]. As a result, the intracellular organization can be disrupted and these transformations can affect the viscoelastic behavior of cells which has been linked with the onset and progression of marked pathologies[27], [32].

A variety of approaches exist for detecting oxidative stress such as immunological based techniques (i.e. ELISA, Western blot), fluorescence, electron-spin resonance, nuclear magnetic resonance, mass spectrometry, as well as ROS detection probes[12], [33]. Such techniques provide valuable information but are often limited in that they are typically destructive, expensive and often detect the result of downstream oxidative events (i.e. lipid, protein, or DNA oxidation). Oxidative damage on intact cells can be evaluated by measuring morphology and viscoelastic properties of cells using techniques such as optical tweezers, particle tracking microrheology, micropipette aspiration, magnetic tweezers and magnetic twisting cytometry[34]–[36]. Nevertheless, operation of these techniques might necessitate external interventions that can damage the cellular structure; for instance, applying external force during cell poking or local heating due to manipulation of cells using light. Techniques such as micropipette aspiration cause deformation of cell body and has limited spatial resolution. Additionally, approaches involving magnetic tweezers and magnetic cytometry use particle embedding in cells which can only detect elastic responses. Even though the aforementioned techniques are informative, they are end-point assays and provide information at an instance of time of the cellular redox and biophysical state[27], [36].

Conversely, quartz crystal microbalance with dissipation (QCM-D) has become an attractive technique for measuring the real-time and in situ changes in mass and viscoelastic properties of biological films[37]. This acoustic surface-sensitive technique measures changes in mass near the sensor surface as a shift in the resonance frequency ($\Delta f$-response) of the sensor crystal and changes in viscoelastic properties of the adhered film is measured as the changes in the energy dissipation ($\Delta D$-response) of the sensor shear oscillation[38], [39]. Previous studies using different cell-lines have shown that QCM-D can detect cell adhesion and cell spreading by

generating distinct Δ*f*- and/or Δ*D*-response curves under the same experimental set-up[40], [41]. This technique has also been used for real-time and in situ treatments of adhered cell monolayer with different perturbing agents, where Δ*f*- and Δ*D*-responses were monitored and linked to changing viscoelastic behavior of cells due to their interactions with external agents or with functionalized sensor surfaces. In this work, QCM-D was used to investigate the effects of oxidative stress induced by exposure of MC3T3 cells, a pre-osteoblast murine cell-line[42], to various concentrations of $H_2O_2$. Previous studies using pre-osteoblast cells have indeed demonstrated that the event of oxidative stress inhibited mineralization and differentiation of MC3T3 cells in vitro conditions[19], [43]. Additionally, in vivo studies have shown that oxidative stress can lead to increased inflammatory cytokine levels in bones which eventually leads to diseases such as osteoporosis[44].

In this study, we used QCM-D to measure the real-time and *in situ* effects of $H_2O_2$ on the viscoelastic properties of MC3T3 cells. With 30 min incubation period, we observed that there was a recovery in dissipation signal for 25 M μM $H_2O_2$, and hence, we took interest in studying the effects of other $H_2O_2$ concentrations on the adhered MC3T3 cell monolayer when incubated with $H_2O_2$ for 30-min period. Pre-osteoblast MC3T3 cell-line was chosen as per the author's interest in bone tissue engineering. Each QCM-D experiment was performed for a total time of 350 min (Figure 1 and 2) and this time limit was not exceeded to avoid effects due to lack of sterility. The Δ*D*-response curves obtained show a clear $H_2O_2$ concentration dependence on the viscoelastic properties of cells, where the sensor surface with adhered cells becomes more rigid with increasing $H_2O_2$ concentration. We confirm using fluorescence microscopy, scanning electron microscopy (SEM) and atomic force microscopy (AFM), along with standard biochemical assays, namely, cell viability and total antioxidant capacity (TAC), that the changes

in viscoelastic properties observed by QCM-D are indeed the result of $H_2O_2$-induced oxidative stress.

## 2. MATERIALS AND METHODS

### 2.1. Cell culture

All cell culture work was performed in a Class II Biological Safety Cabinet using standard aseptic cell-culture handling techniques. The MC3T3 cell line (ATCC, Virginia, USA) was maintained in a cell culture incubator (5% $CO_2$, 37$^o$C, Microzone Corporation, ON, Canada) and was cultured in sterile T75 cell-culture flasks (Greiner Bio-One, Frickenhausen, Germany) with vented caps in alpha-minimum essential medium (MEM-alpha, Invitrogen, California, USA) supplemented with 10% fetal bovine serum (Neuromics, Minnesota, USA) and 1% of penicillin-streptomycin (Invitrogen). Cell passages between P13 and P19 were used to avoid passage-induced variation. At 85-90% confluency, cells were trypsinized (using 0.05% trypsin in EDTA solution, Invitrogen) from the cell-culture flask and centrifuged (300g, 5 min). MC3T3 cells were then seeded at 250,000 cells/ml onto poly-D-lysine-(PDL) coated polystyrene quartz crystal sensor (14mm diameter) or PDL-coated round coverslips (~15mm diameter). The sterile PDL (Sigma-Aldrich, Missouri, USA) coating was used to ensure strong adhesion of the MC3T3 cells to the surface. Each sensor or coverslip was placed in a single well of a 12-well plate (Thermo Fisher Scientific, Massachusetts, USA). The well-plate was then placed in a cell-culture incubator (5% $CO_2$ and 37$^o$C) for 24h prior to any experiment to obtain an adhered confluent cell monolayer film on each sensor or coverslip. Each sample was prepared in triplicate.

### 2.2. QCM-D measurements

Polystyrene-coated (PS, QSX 305, Biolin Scientific, Gothenburg, Sweden) AT-cut 5MHz quartz crystals in the form of 14mm-disks were used as the QCM-D sensors. The PS sensors

were cleaned according to the manufacturer's guidelines (Biolin Scientific). Briefly, sensors were stored in 1% Deconex solution at 30ºC for 30 min and then immersed in Milli-Q $H_2O$ for at least 2h. The sensors were then rinsed with Milli-Q $H_2O$ prior to rinsing in 99% ethanol, dried under nitrogen gas, and exposed to UV light for 15 min before coating with sterile PDL solution overnight. MC3T3 cells were seeded onto the sensors for 24h prior to any further experiment. Before carefully mounting the sensors onto the flow chambers, and to ensure minimal disruption of the adhered cells, the sensors were imaged under the light microscope to confirm cell attachment to the sensor.

The QCM-D instrument (Q-Sense E4, Biolin Scientific) was used to record changes in frequency ($\Delta f$-response*)* and energy dissipation ($\Delta D$-response) as a function of time at the 3rd overtone (n=3). Prior to QCM-D experiments, each PDL-modified sensor with attached cell monolayer was mounted onto an individual clean flow-module which was placed inside a chamber. The temperature inside the 4-flow-module chamber was stabilized to 37ºC ± 0.02°C. All the solutions were equilibrated to 37ºC in a water bath before being introduced into the chamber. The serum-free medium (SF-medium) which was used as the control for the QCM-D experiment was degassed in a sonicator at 37 ºC to avoid formation of gas bubbles during flow within the chamber. The QCM-D measurements were performed under flowing conditions at 100 µl/min until the final washing step and then reduced to 7 µl/min for the rest of the experiment. Before recording the QCM-D measurements, a conditioning step was employed in which the MC3T3 cell monolayer film was subjected to continuous flow of buffer medium at 100 µl/min for 60 min. This step was performed to ensure that cells stabilized to the flowing conditions at 100 µl/min. Following, $\Delta D$-response curves were recorded using an optimized QCM-D protocol for 350 min. This time limit was not exceeded to avoid non-sterile conditions optimized in this

study[45]. The protocol established for the QCM-D experiments was as follows (Figures 1 and 2): (1) Baseline: Serum-free medium (SF-medium) was injected into the flow chamber for 5 min to obtain a stable baseline at 100 µl/min. (2) ROS treatment: The cell monolayer was then exposed to the $H_2O_2$ concentration of interest, or SF-medium (control), for 5 min under flowing conditions at 100 µl/min. (3) Incubation: The cell monolayer was then incubated in $H_2O_2$ solution or SF-medium (control) for 30 min. (4) Rinsing: Cells were washed with buffer medium to remove the excess material and oxidative products in the chamber for 5 min at 100 µl/min. (5) Monitoring: Shifts in $\Delta f$- and $\Delta D$-response curves were monitored for the rest of the experiment time at 7 µl/min to observe the changes in the cell monolayer mass and viscoelastic properties post-ROS treatment. At least 3 independent experiments were conducted for each condition. For data analysis, an average of three replicates of the $\Delta D$-response curves obtained for each $H_2O_2$ concentration was plotted.

Since the change in dissipation ($\Delta D$-response*)* is a ratio of energies, it is a dimensionless quantity and is reported as $10^{-6}$ dissipation units. At the end of each QCM-D experiment, the sensors were removed from the flow modules and a cell viability assay was performed on cells attached to the sensors (details provided in section 2.3.1). Additionally, light microscopy (Nikon ECLIPSE TE2000-U, NY, USA) was used for observing changes in cell morphology and cell density.

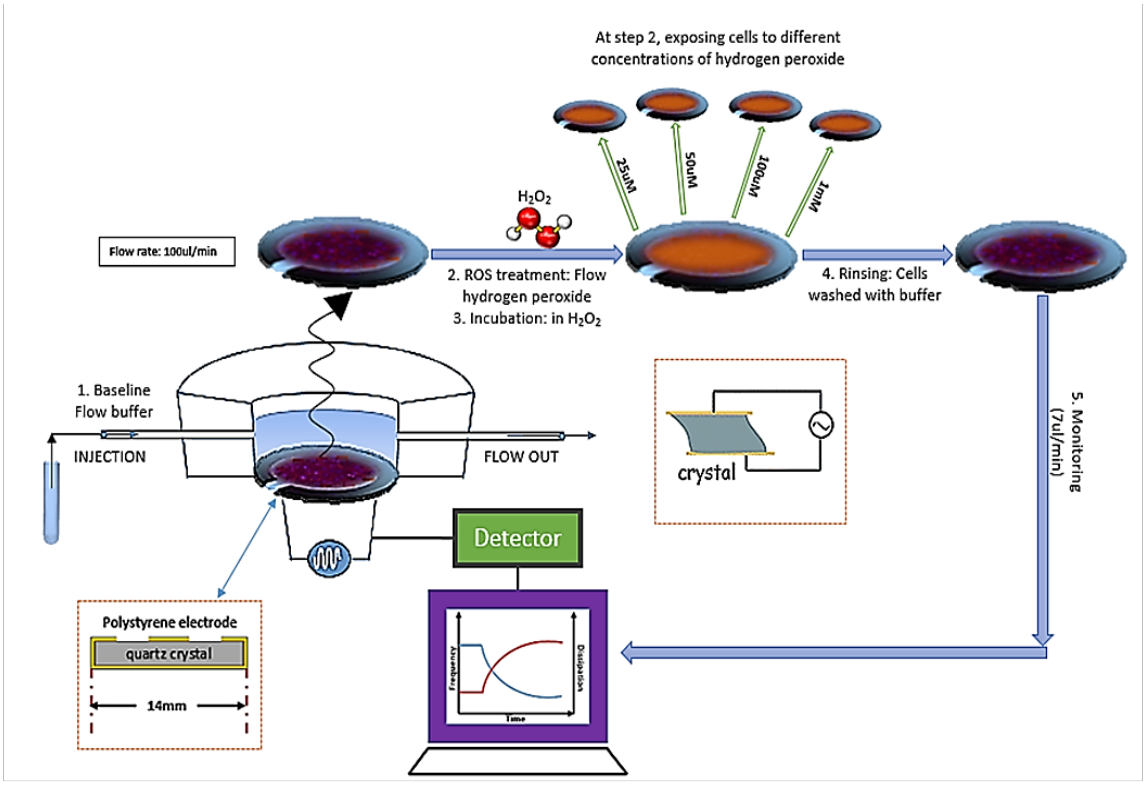


**Figure 1**. Schematic illustration of the QCM-D experimental set-up for studying the effects of oxidative stress on MC3T3 cell-line.

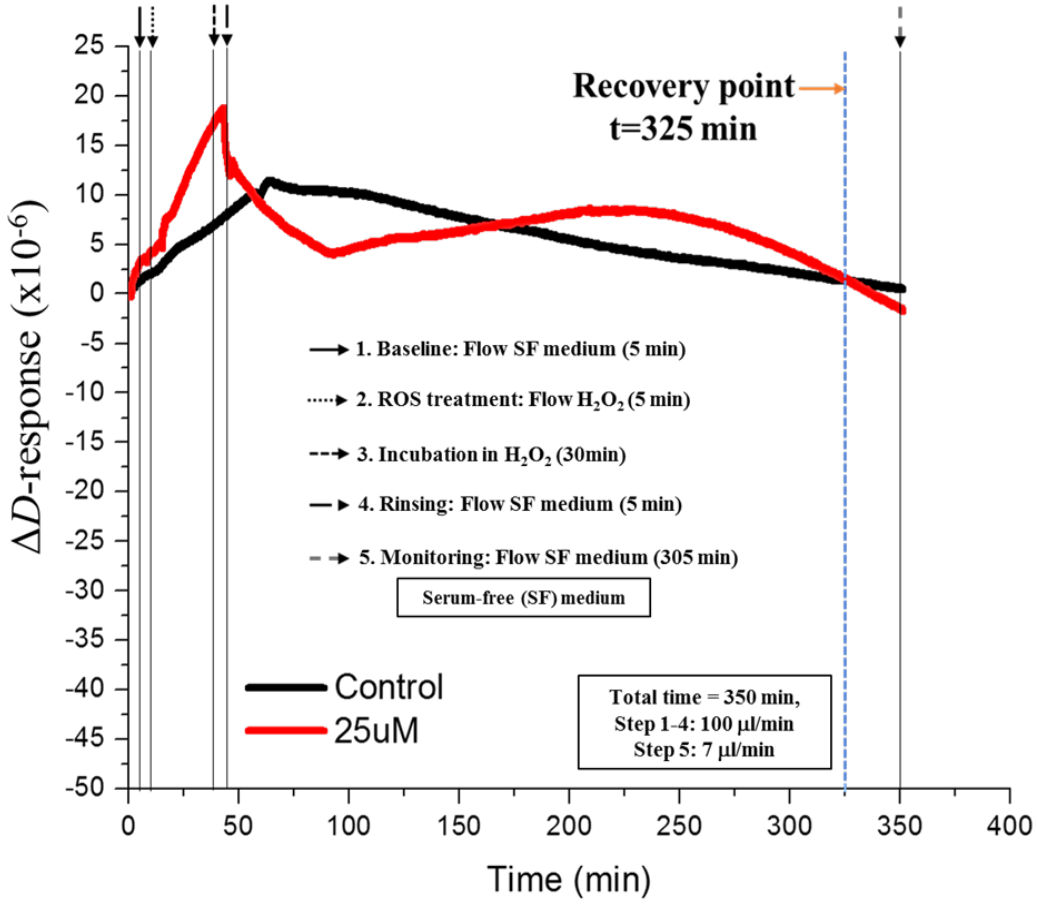


**Figure 2.** Representation of the utilized QCM-D protocol steps and associated Δ*D*-responses generated due to the interaction of MC3T3 cell monolayer with serum-free (SF) medium and 25 µM $H_2O_2$ (an arrow indicates the end of each step).

### 2.3. Microscopy techniques

For imaging techniques such as SEM, AFM and fluorescence (stained actin cytoskeleton and nuclei), initial cell sample preparation steps were as follows: Cell monolayer attached on each PDL-modified coverslip was treated with different concentrations of $H_2O_2$, ranging between 0mM and 10 mM. The established QCM-D protocol was used to prepare the samples in a static condition. Briefly, a cell suspension of 250,000 cells/ml was seeded onto PDL-coated round coverslips for 24h in a cell culture incubator at 37°C and 5% $CO_2$. Cell culture media was then replaced with SF-medium in each well for 65 min. Following, the cell monolayer was incubated

in $H_2O_2$ for 35 min and washed with SF-medium for 5 min (removal of $H_2O_2$). For associating the $\Delta D$-response curves with changes in the cell morphology, another set of cells were allowed to incubate in SF-medium until the recovery point (t=325 min). The cells were then fixed using 4% paraformaldehyde (ACROS Organics, NJ, USA) for 30 min and then rinsed twice with phosphate–buffered saline solution (PBS, BioShop, ON, Canada).

**2.3.1. Fluorescence imaging**

Fluorescence imaging was used for two purposes: (a) Live/dead cell imaging: After the QCM-D experiments, each sensor with adhered cell monolayer was incubated with 2 μM calcein and 4 μM ethidium homodimer-1 solutions at room temperature for 30 min using the LIVE/DEAD™ Viability/Cytotoxicity kit for mammalian cells (#L3224, ThermoFisher Scientific). Each sensor was placed in a single well of a 12 well-plate. Calcein (Excitation/Emission = 494/517 nm) is a cell-permeant reagent that is converted into its green fluorescent form by intracellular esterase activity inside living cells. Ethidium homodimer-1 (Excitation/Emission = 528/617 nm) can only enter damaged cell membrane and upon binding with nucleic acids it irradiates red fluorescence. Reagent solutions were pipetted carefully to completely cover the top of the sensor and ensure minimal disruption of the residual cell monolayer. After staining, sensors were imaged on a fluorescence microscope and images were captured (Nikon ECLIPSE TE2000-U) using the NIS Elements D (v4.11.00) software. The central region of the sensor was imaged as it is the most responsive area and the images were captured using 10X magnification. An image processing software (Schindelin, J.; Arganda-Carreras, I. & Frise, E. et al. (2012), "Fiji: an open-source platform for biological-image analysis", Nature methods 9(7): 676-682, PMID 22743772, doi:10.1038/nmeth.2019) was used to superimpose the live cell and the dead cell images from the same region of the sensor surface

and for the live/dead cell ratio analysis. To count the live and dead cells, we employed a methodology for image processing described in details elsewhere[46].

For observing cell cytoskeleton and nucleus, cell samples were washed with Triton X-100 solution (1:10000 in PBS), PBST (1 drop of tween in 50 ml PBS + tween) solution and subsequently with 3% bovine serum albumin (BSA). For phalloidin and hoechst staining, fixed samples were first treated with Alexafluor 647 Phalloidin (#A22287, Molecular Probes, Oregon, USA) at a concentration ratio of 3:10 in PBS at room temperature for 20 min and then were treated with hoechst fluorescent nucleic acid stain (#33342, ImmunoChemistry Technologies, MN, USA) at a concentration of 1:200 in PBS at room temperature for 20 min. The round coverslips with stained samples were mounted on glass slides using a mounting medium (Aqua-Mount, ThermoFisher Scientific). Fluorescence images were collected using an inverted confocal microscope (Zeiss LSM 710, Oberkochen, Germany) at 63x magnification and image processing was performed using Zen 2 (blue edition) software.

**2.3.2. Scanning Electron Microscopy**

The samples obtained after the removal of $H_2O_2$ and recovery point were fixed using 4% paraformaldehyde, dehydrated using a series of ethanol solutions (increasing the ethanol concentration from 30% to 100%, diluted accordingly with Milli-Q $H_2O$) and critical-point dried with $CO_2$ (CPD030, Leica Microsystems Critical Point Dryer, Ontario, Canada). Critical-point dried samples were mounted on aluminum pin stubs and sputter-coated with a 5nm layer of platinum (Leica Microsystems EM ACE600 High Resolution Sputter Coater). The samples were imaged using field emission gun scanning electron microscopy (FEI Inspect F50 FE-SEM, ThermoFisher Scientific) at an accelerating voltage of 5kV. An image processing software (refer to section 2.3.1) was used to process and analyze the SEM images.

### 2.3.3. Atomic Force Microscopy

The cell samples harvested after the removal of $H_2O_2$ and recovery point were fixed with 4% paraformaldehyde and dehydrated using a series of ethanol solutions (increasing the ethanol concentration from 30% to 100%, diluted accordingly with Milli-Q $H_2O$). The samples were then allowed to air dry at room temperature (~20 min). Dry conditions were used to ensure cell preparation procedure similar to SEM studies. The samples were then imaged using a Nanoscope IIIa AFM (Digital Instruments, California, USA) with a silicon probe (75 kHz resonant frequency, force constant 2.8 N/m, ARROW-FMR-10, S/N: 70596F14L902, NanoWorld Innovative Technologies, Neuchâtel, Switzerland) operating in tapping mode. AFM Images were generated using Nanoscope software (v5.12r5). A range of scan rate was used to image all the AFM samples: 0.2 Hz - 0.4 Hz and 0.7 Hz for 10 mM sample only. It is to be noted that the scan rate was adjusted because the viscoelasticity differed among each sample due to varying $H_2O_2$ concentration treatment and a fixed scan rate could not be utilized due to artifacts during imaging of some of the samples.

### 2.4. Total Antioxidant Capacity (TAC)

*Cell-lysate preparation*

Approximately 100,000 MC3T3 cells were cultured in a cell-culture flask with vented caps in supplemented MEM-alpha until 80-95% confluency was reached. The culture medium was then replaced with SF-medium for 65 min and then cells were treated with the $H_2O_2$ concentration of interest for 35 min. Using a rubber policeman, adherent MC3T3 cells were harvested after washing with SF-medium for 5 min or at recovery time point (t=325 min), and then centrifuged (2000g, 10 min, 4$^{o}$C). After centrifugation, the supernatant was removed and the cell pellet was rinsed in PBS twice. Following centrifugation, the cell suspension was

transferred to accurately weighted and labelled micro-centrifuge tubes and then centrifuged (2000g, 10 min, 4$^{o}$C). The supernatant was removed, and the mass of each pellet was measured. The samples were then stored at -80$^{0}$C overnight after flash freezing in liquid nitrogen. Frozen cell pellets were thawed on ice and then re-suspended in 500 µl of cold buffer (5 mM potassium phosphate, pH 7.4, containing 0.9% sodium chloride and 0.1% glucose). Cell lysates were prepared by sonication using a microtip sonication probe. Samples were kept in an ice/water bath during sonication for 5 secs and then centrifuged (10,000 g, 15 min, 4$^{o}$C). The supernatant was collected for TAC measurements.

*Sample preparation*

The TAC experiments were conducted using an Antioxidant Assay Kit (#709001, Cayman Chemical, Michigan, USA). Reagents provided in the kit were metmyoglobin, chromogen and $H_2O_2$ working solution. The procedure provided in the kit was followed. Briefly, 10 µl of sample was added to 10 µl of metmyoglobin and 150 µl of chromogen in each well of a clear 96-well plate. Each of the cell lysates analyzed were measured independently with a minimum of three replicates per lysate. A multi-channel pipette was used to simultaneously deliver 40 µl of $H_2O_2$ working solution into each well. After exactly 30 secs, a plate reader (SpectraMax i3, Molecular Devices, CA, USA) was used to measure the absorbance at 750nm ($A_{750}$). Each absorbance reading was used to calculate the total antioxidant concentration in each sample and the value was divided by the mass of cell sample in each respective micro-centrifuge tube. Statistical analysis was conducted using two-way ANOVA test with GraphPad Prism 8.0.0 version software.

# 3. RESULTS

## 3.1. QCM-D measurements - Δ*D*-responses induced by oxidative stress

Stable Δ*f*- or Δ*D*- baselines were first obtained for all the experiments before adding $H_2O_2$. We performed three control experiments to ensure that Δ*D*-response curves exclusively report the interaction between MC3T3 cells and $H_2O_2$ only (Figure 3-A, 3-B, and S1-A). No large effect on Δ*f*- or Δ*D*-response was observed when PDL-coated sensors were subjected to either serum-free medium, referred to as SF-medium in this paper (Figure 3-A) or 10 mM $H_2O_2$ (Figure 3-B). By contrast, both Δ*f*- or Δ*D*-response curves exhibited a very sharp upward increase and downward decrease respectively, when cells were exposed to 10% bleach solution (Figure S1-A). Figure 3-C shows the Δ*D*-response curves generated due to varying $H_2O_2$ concentration treatment on the adhered monolayer of MC3T3 cells. The first key observation was that each $H_2O_2$ concentration treatment resulted in a unique Δ*D*-response curve. Secondly, it was evident that for $H_2O_2$ concentrations > 25 μM, the higher the concentration, the greater the decline in the Δ*D*-response curve, which is indicative of changes in the viscoelastic properties of the adhered cell monolayer – increasing sensor surface rigidity with increasing concentration. Interestingly, for the lowest concentration tested, which was 25 μM $H_2O_2$, we observed that the Δ*D*-response curve, following dramatic changes, returned close to the baseline values and intersected with the control Δ*D*-response curve. This intersection point gained the author's interest and was marked as the recovery point (t=325 min).

After obtaining a baseline for 5 min, upon the addition of $H_2O_2$ solution, a common trend was observed between the Δ*D*-response curves of the $H_2O_2$ concentration tested. Each curve exhibited a sharp rise, reached a peak point and then declined dramatically. For the 25 mM, following the initial decline, a slow and gradual rise in the Δ*D*-response curve was observed

followed by a gradual decline. Although 25 mM Δ*D*-response demonstrated recovery, for the remaining concentrations tested (50 μM-10mM), no recovery was observed. For the 100 mM $H_2O_2$ Δ*D*-response, a second lower peak was observed following which there was a dramatic decline and then a slow rise. 1 mM Δ*D*-response curve exhibited a very small drop after the first peak which was followed by a short period of fluctuations and then a downward decrease after the removal of $H_2O_2$. On the other hand, 10 mM Δ*D*-response curve exhibited the fastest initial peak as compared to the Δ*D*-response of other $H_2O_2$ concentrations. A very small peak was observed at the point of removal of 10 mM $H_2O_2$, which then quickly declined exhibiting a significant rapid decrease until a plateau was reached toward the end of the experiment. Interestingly, the rate of upward rise, the peak point and the rate of decline of the Δ*D*-response curves differed among each concentration treatment with 50 μM $H_2O_2$ generating the highest peak after the removal of $H_2O_2$. Extending our observations, we saw that for concentrations > 50 mM, the initial upward rise, the first peak point and decline in the Δ*D*-response curves occurred before the removal of $H_2O_2$. Finally, at the recovery time point (t=325 min), we observed that the higher the concentration, the greater the magnitude of the Δ*D*-response. The $H_2O_2$ concentration-dependency was further assessed by calculating a line of best fit for the magnitude value of the Δ*D*-response curves at the recovery point (Figure S2-B). For this purpose, we converted the concentration values to a logarithmic scale. As demonstrated, there is an inverse linear relationship between the magnitude of Δ*D*-response and the $H_2O_2$ concentration at the recovery point (Figure S2-B). For the control group, the Δ*D*-response curve initially exhibited a gradual upward increase and then slowly declined until the end of the experiment. Since all the experiments were completed within 6 hours, non-sterile conditions were not a concern [45]

which was confirmed when the MC3T3 cell monolayer with no $H_2O_2$ treatment was found to be confluent and healthy after the QCM-D experiment (Figure S2).

Δ*f*-response generated due to MC3T3 cell monolayer exposure to $H_2O_2$ demonstrated distinct curves for every concentration tested (Figure S1-C). For concentrations 50 mM and 10 mM, we observed rapid fluctuations in the respective Δ*f*-response curves for the first 75 min and then the curves became steady. For 1 mM $H_2O_2$, the Δ*f*-response exhibited a slow upward rise following short fluctuations. For 25 mM and 100 mM, the Δ*f*-response curves demonstrated small fluctuations near the baseline. The control group exhibited an interesting and different behavior as compared to other concentrations. We observed that the control Δ*f*-response curve declined gradually until the end of the experiment. However, even though these changes were detected, unlike the Δ*D*-response, the Δ*f*-response shows no $H_2O_2$ concentration-dependency (Figure S1-C) and also, there was no similar trend observed between the Δ*f*-response curves for all the concentrations tested. Since the Δ*f*-response mainly detects the changes in the small, localized basal region of the cells[47], we decided to focus on the Δ*D*-response for investigating the effects of oxidative stress on the viscoelastic properties of MC3T3 cell monolayer.

Light microscopy images of the sensors after QCM-D measurements showed a reduction in cell density as $H_2O_2$ concentration increased. Cell morphology also appeared to be less spread as compared to the control cells (Figure S2). Additionally, cell viability of MC3T3 cells adhered to the polystyrene sensors after QCM-D measurements confirmed that with increasing $H_2O_2$ concentration, percentage of live cells decreased and dead cells increased (Figures 3-D and S1-D). Moreover, a significant decrease in live/dead cell ratio for $H_2O_2 > 25$ μM was detected (Figure S1-E and F).

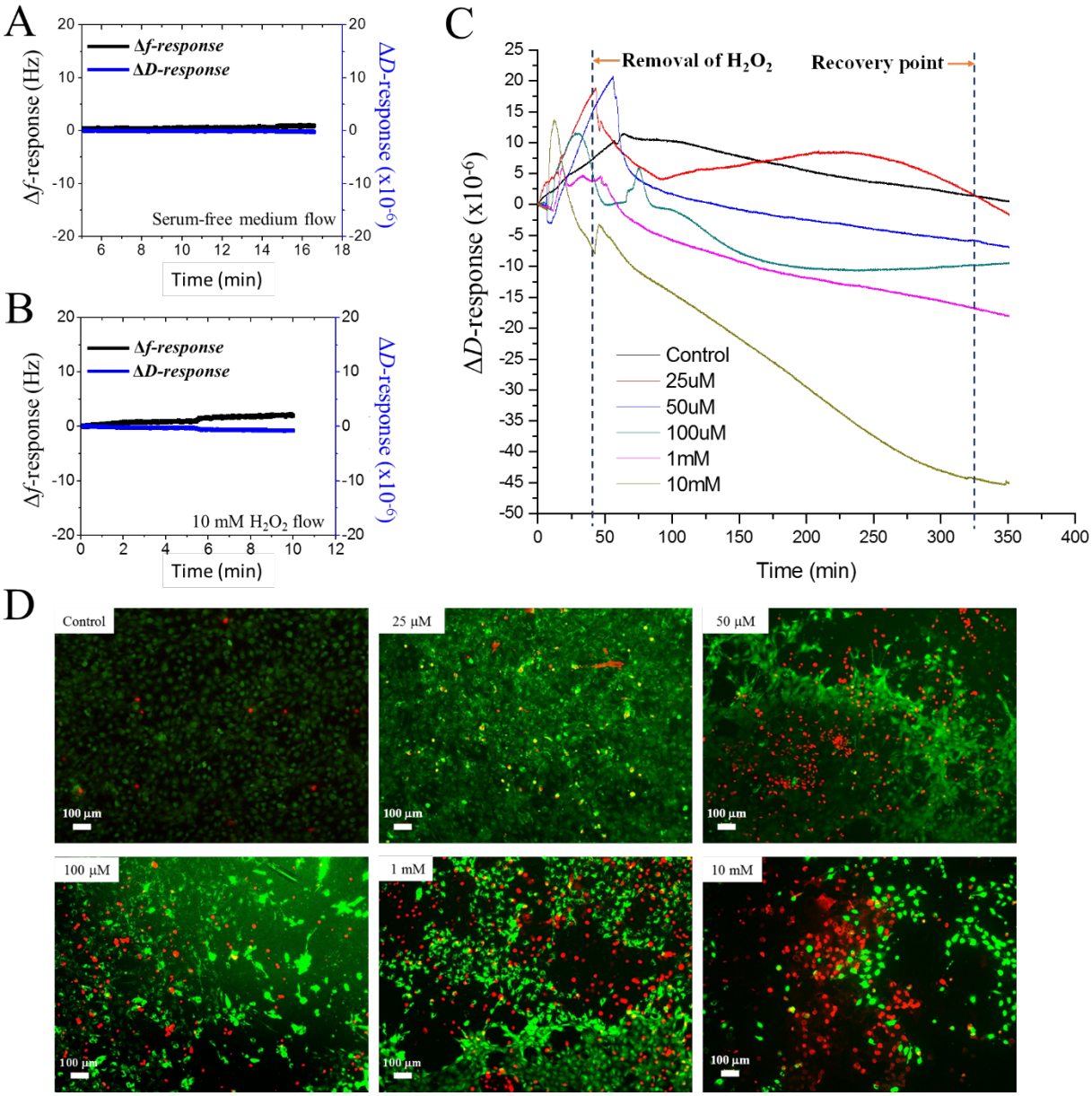


**Figure 3.** Real-time QCM-D measurements of (A and B) Δ*f* and Δ*D*-responses obtained from exposure of PDL-coated polystyrene quartz sensor to buffer medium for about 17 min and to 10 mM $H_2O_2$ for about 10 min, respectively, and (C) Δ*D*-responses of MC3T3 cell monolayer to $H_2O_2$ for 350 min. Distinct Δ*D*-response curves were generated for cellular response to each $H_2O_2$ concentration treatment. For $H_2O_2$ > 25 μM, the higher the concentration, the more the decline in the Δ*D*-response curve. Recovery in Δ*D*-response was obtained with 25 μM $H_2O_2$, whereas no recovery was observed for other concentration treatments. The control experiments (A and B) confirmed that the Δ*D*-responses resulted only due the interaction between the cells and $H_2O_2$. (D) Images of live/dead assay conducted on cells adhered to sensors post QCM-D experiments show reduction in cell viability with increasing $H_2O_2$ concentration (live = green; dead = red).

### 3.2. Correlation of the $H_2O_2$-induced Δ*D*-response with restructuring of actin cytoskeleton and cellular health

The $H_2O_2$-induced changes in the actin cytoskeletal structure of MC3T3 cells after the removal of $H_2O_2$ revealed a concentration-dependent effect on the cytoskeleton (Figure 4-A). $H_2O_2$ concentrations > 50 μM induced shrinkage and retraction of the cytoskeletal structure and also, led to apoptotic cells. On the other hand, with 25 μM $H_2O_2$ concentration treatment, the average nucleus size slightly increased, the actin structure appeared slightly shrunk and the cellular bodies appeared to be more spread out as compared to the untreated cells. Few cells also demonstrated signs of early apoptotic stage. Cells treated with $H_2O_2$ concentration between 50 μM and 1 mM exhibited clear condensed and pyknotic nuclei, while few other cells demonstrated fragmented nuclei. This shows that with $H_2O_2$ treatment between 50 μM and 1 mM, majority of the stressed cells were apoptotic with few necrotic cells. This phenomenon was not distinguishable for MC3T3 cells exposed to 10 mM $H_2O_2$, since they exhibited a typical necrotic morphology. With increasing concentration, shrinkage in F-actin cytoskeletal structure occurred and the cytoskeleton completely diminished with $H_2O_2$ treatment > 1 mM. The average nucleus area (Figure 4-B) shows that 25 μM $H_2O_2$ led to slight increase in nucleus size similar to results reported by Kiyoshima et.al[15], and the smallest nuclear area was obtained with 10 mM $H_2O_2$.

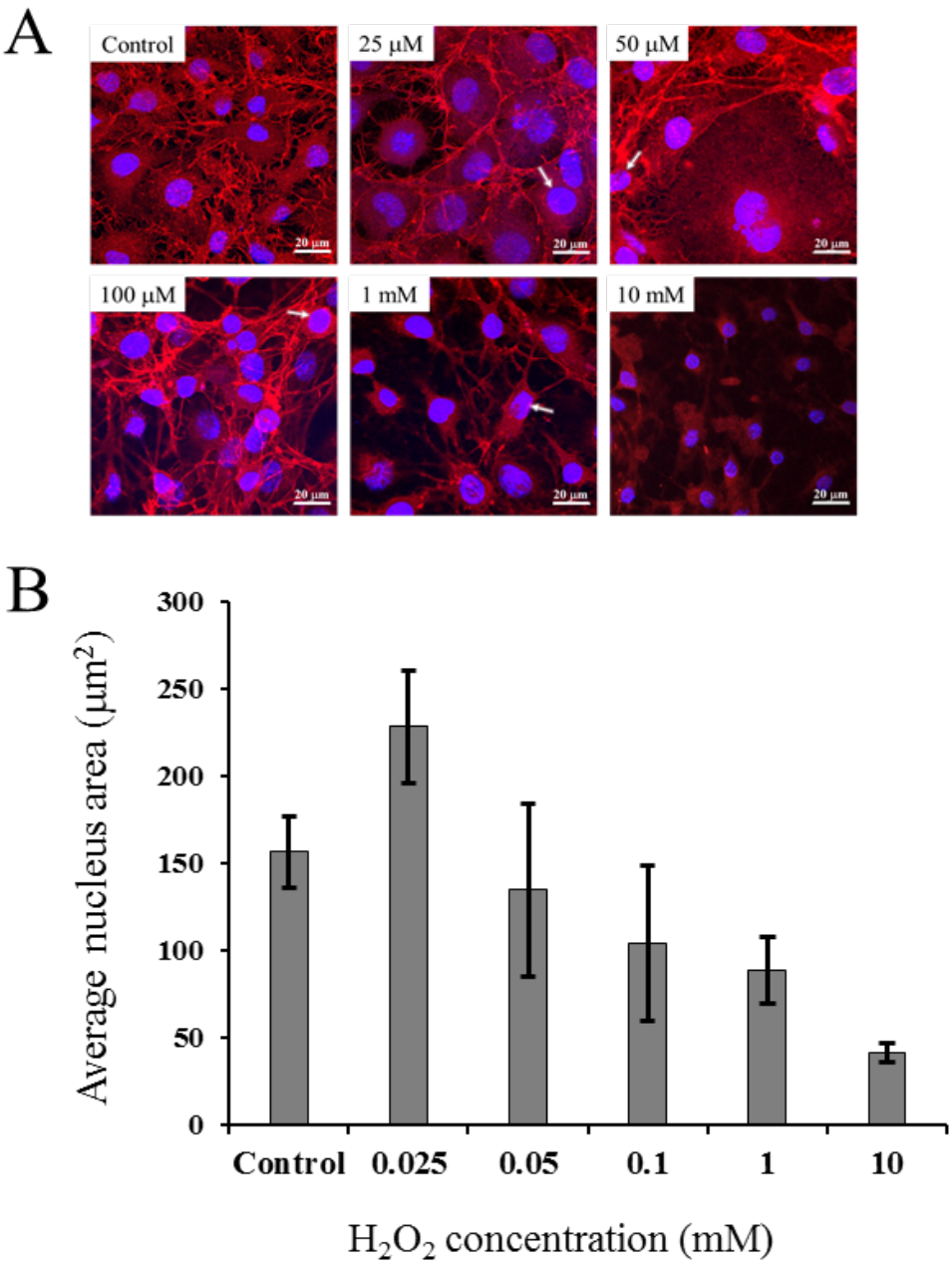


**Figure 4.** (A) Fluorescence images showing stained actin cytoskeleton (red) and nuclei (blue) of MC3T3 cells after removal of $H_2O_2$. 25 µM $H_2O_2$ concentration treatment led to slight increase in the size of the nuclei while the actin cytoskeleton appeared similar to the control cells. With increasing concentration, shrinkage of actin cytoskeleton, and nuclear condensation and fragmentation (example indicated by white arrows) were evident indicating apoptotic cells, whereas, with 10 mM $H_2O_2$ treatment most cells appeared to be necrotic with diminished actin cytoskeleton. (B) Bar graph represents average area of nucleus of MC3T3 cells (n=5) due to each $H_2O_2$ concentration treatment with 10 mM concentration treatment resulting in the smallest nucleus area.

### 3.3. Assessing the cell morphology using Scanning Electron Microscopy:

SEM observation of cells treated with 25 μM $H_2O_2$ and fixed after the removal of $H_2O_2$ presented flattened morphology similar to control cells, but their membranes appeared to have small blebs which is characteristic of oxidative stress[16], [47], [48] (Figure 5-A). For the $H_2O_2$ > 25 μM, the morphological changes were more evident due to visible alteration in the lateral and apical surfaces of the cell membrane. Furthermore, the $H_2O_2$-induced apoptotic damage of MC3T3 cells was characterized by the formation of protrusion, small and large blebs, cell body shrinkage, rounding, and irregular cell body shape. MC3T3 cells treated with 10 mM $H_2O_2$ exhibited membrane disruption and membrane wrapped-fragments. At the recovery point (Figure 5-B), cells treated with 25 μM $H_2O_2$ seemed to regain their regular morphology when compared to the control cells. For $H_2O_2$ >50 μM, morphological alterations persisted evidenced by the presence of blebs and rounded cells as compared to the control cells. The spindle-like shaped cells and retracted actin cytoskeleton network were found for the recovered cells treated with 100 μM concentration, indicating permanent damage to cells. Finally, body shrinkage, destruction of actin fibers, protrusion, small and large blebs on surface of cells, and membrane rupture were fatal to cells after treatment with 10 mM $H_2O_2$. Interestingly, AFM studies (Figure S3) showed that as the concentration of $H_2O_2$ treatment increases, the average lateral distance of individual cell decreases. However, for 25 μM $H_2O_2$, the average lateral distance of cells recovers to a value close to the control cells at the recovery point.

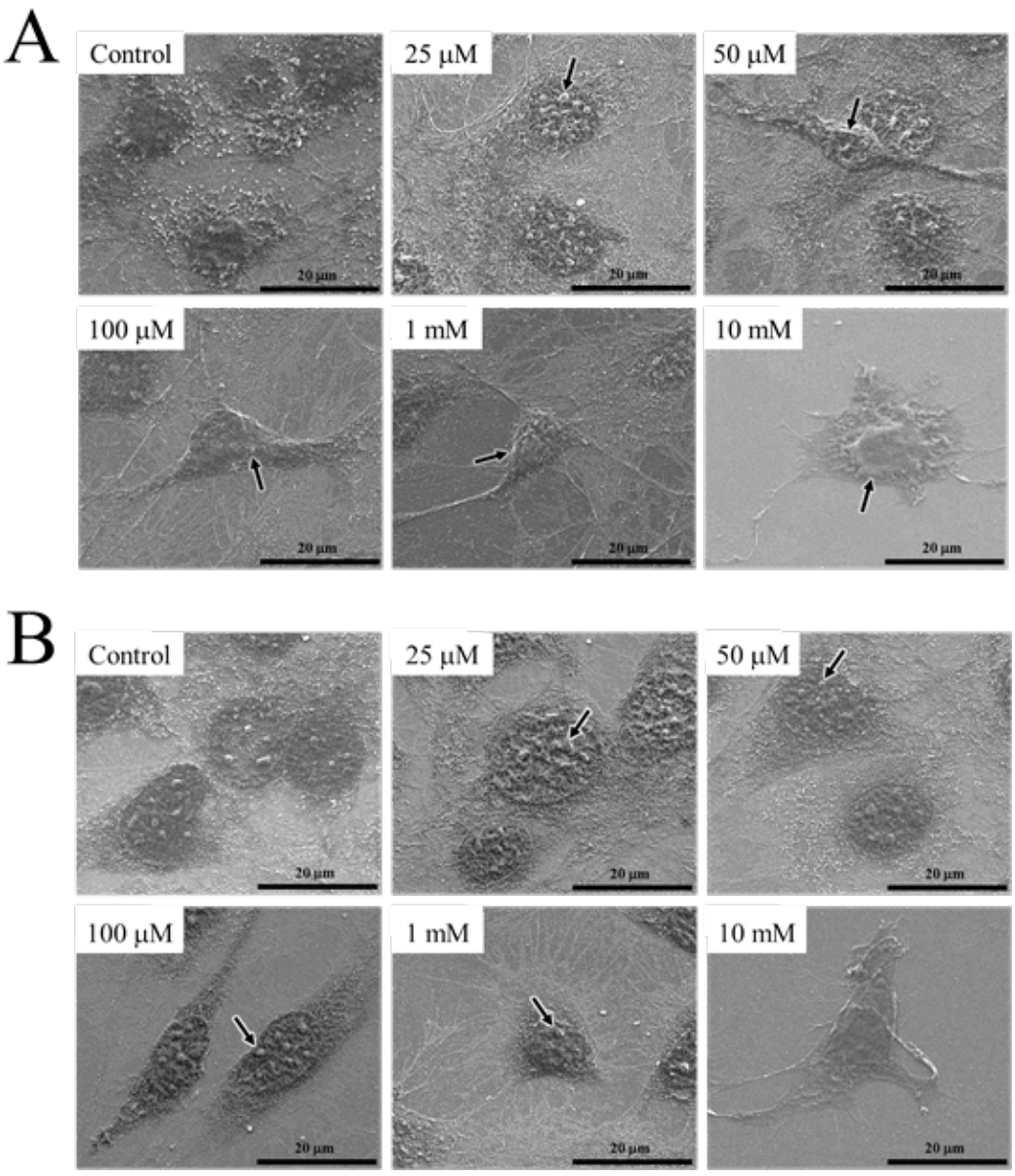


**Figure 5.** SEM images showing the effects of varying concentrations of $H_2O_2$, on the morphology of MC3T3 cells fixed after (A) removal of $H_2O_2$ and (B) recovery point. The imaging results revealed that after the removal of $H_2O_2$ solution, cells treated with 25 µM exhibited an extended morphology similar to control cells, whereas with increasing $H_2O_2$ concentration, oxidative damage was characterized by small and large bleb formation (indicated by black arrows), irregular morphology, rounding of cells, membrane breakdown and cell body shrinkage (10 mM). At recovery point, cells treated with 25 µM seemed to have regained their normal morphology, whereas cells treated with higher concentrations exhibited surface blebs, altered morphology, ruptured membranes and membrane- wrapped fragments (10 mM) indicating apoptotic/necrotic behavior (Surface area represented for each image ~ 0.003 $mm^2$)

### 3.4. Evaluation of total antioxidant capacity (TAC) of $H_2O_2$-treated cells

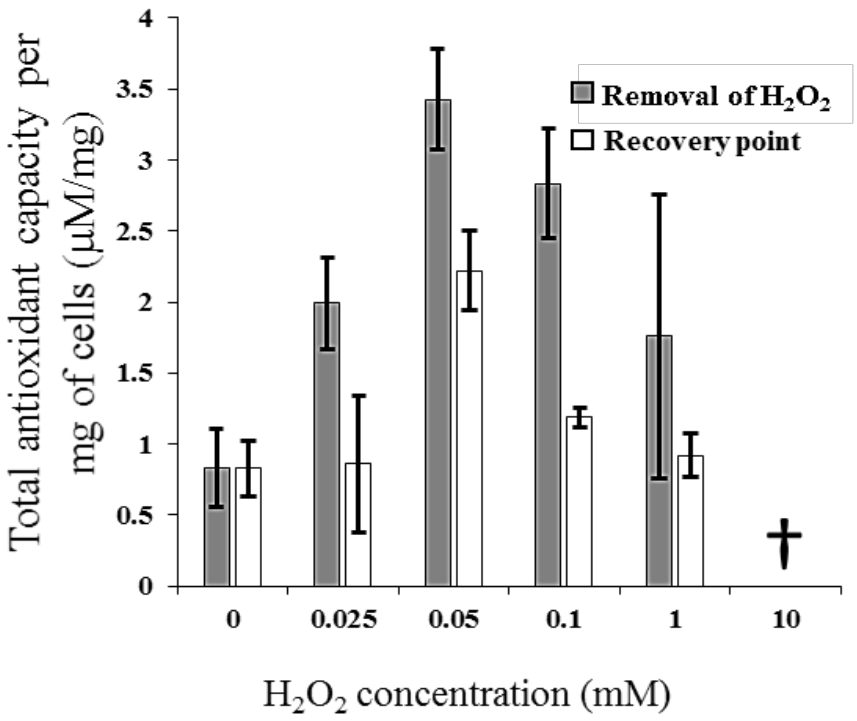


**Figure 6.** Bar graph representing total antioxidant capacity of cells per mg after the removal of $H_2O_2$ and at the recovery point. A parabolic trend was observed in antioxidant levels with increasing $H_2O_2$ concentration treatment and peak level was obtained with 50 µM $H_2O_2$ treatment. At recovery point, there was reduction in antioxidant levels for all the concentration treatment and cells treated with 25 µM $H_2O_2$ displayed recovery in antioxidant levels close to the control cells ($P>0.9999$, $n=3$) which indicates recovery from oxidative stress. † 10 mM $H_2O_2$ treatment produced very low antioxidant levels which fell outside the detection range and hence, could not be determined by this assay.

TAC assay indicated that after the removal of $H_2O_2$, the antioxidant levels in cells increased with increasing $H_2O_2$ concentration until up to 50 µM $H_2O_2$ treatment which was followed by a decline in the antioxidant levels for $H_2O_2 > 50$ µM (Figure 6). Notably, the TAC per mg of cells treated with 10 mM $H_2O_2$ could not be detected and fell below the limit of detection (<0.33 mM) for the TAC assay kit employed. After the removal of 25 µM $H_2O_2$, the TAC levels detected in cells was about 1.2-fold higher than the control group. For cells treated with $H_2O_2$ concentration up to 1 mM, a recovery in TAC per mg of cells was measured. Interestingly, the TAC per mg of cells measured at the recovery point for the 25 µM $H_2O_2$ treatment was very close to the control

group. Statistical analysis conducted using two-way ANOVA test revealed no significant differences between the TAC levels obtained from control cells and cells treated with 25 μM $H_2O_2$ at the recovery point (Table S1).

A parabolic trend was observed for the TAC levels as a function of the $H_2O_2$ concentration after the removal of $H_2O_2$ which is analogous to the parabolic trend observed for the levels of TAC detected in cells at the recovery point.

## 4. DISCUSSION

In addition to inducing changes in the cell redox state and biochemical pathways, oxidative stress leads to changes in the cytoskeletal structure and cell morphology which influences the viscoelastic properties of cells under stress. The viscoelastic-change response of cells due to oxidative stress results from associated change in biochemical pathways and cellular architecture. Even though various techniques for measuring cellular biomechanics exist, so far, no studies have evaluated the real-time and non-invasive viscoelastic changes in any cell-line due to oxidative stress. Therefore, in this study we have established a powerful sensing platform using QCM-D to exclusively study the oxidative stress-induced changes in cells' viscoelastic behavior. As the distance from the sensor surface increases, the amplitude of shear wave of the oscillating quartz crystal is exponentially dampened. The penetration depth (δ) of the acoustic shear wave of the QCM-D decaying into a liquid coupled to the sensor, is given by:

$$\delta = \sqrt{\frac{\eta}{\pi\rho f}}, \qquad \text{Eqn. 1}$$

where $\boldsymbol{\eta}$ is the viscosity of the liquid, $\boldsymbol{\rho}$ is the density of the liquid, and $\boldsymbol{f}$ is the frequency of the shear wave of the $\boldsymbol{\eta th}$ vibrational mode[37]. For n=3, the acoustic wave has a penetration depth of 100-150nm from the surface of a 5-MHz quartz sensor disk[49]. This depth coincides with the height of the basal region of the cell monolayer which allows QCM-D technique to characterize

the changes in viscoelastic properties of the adhered cell monolayer. The link between Δ*D*-responses, associated signaling pathways and recovery in viscoelastic properties have been shown in previous studies[45], [50]. In this study, the real-time, Δ*D*-response was demonstrated to be a direct and sensitive measure of the time-dependent changes in the convoluted set of properties of adherent MC3T3 cell monolayer, induced by varying $H_2O_2$ concentrations. A $H_2O_2$ concentration-dependent cellular response was revealed by the Δ*D*-response and the control experiments confirmed that the distinct Δ*D*-response curves could only be a result of $H_2O_2$-induced changes in the viscoelastic properties of the MC3T3 cell monolayer.

As seen in Figure 3-C, the changes in 25 μM Δ*D*-response curve followed a similar trend as compared to the other concentrations. However, interestingly, the 25 μM Δ*D*-response curve returned close to the baseline where it intersected with the Δ*D*-response of the control group to which no $H_2O_2$ was added. At this intersection, which was marked as the recovery point (t=325 min), we observed an inverse linear relationship between the magnitude of Δ*D*-response curve and the $H_2O_2$ concentration (Figure S1-B). Since Δ*D*-response is related to the rigidity of the adhered film on the sensor surface, it can be said that for with $H_2O_2 > 25$ μM, with increasing $H_2O_2$ concentration, the overall rigidity of the adhered film increased due to increased stiffness of the cells when compared to the control. The stiffness of the cell is determined by the cytoskeleton[51] and we observed that exposure to $H_2O_2$ led to the alteration in the cell cytoskeletal structure (Figure 4-A), which in turn caused changes in the cell morphology (Figures 5-A and B, and S-3). Moreover, the $H_2O_2$-induced alteration in cell morphology led to changes in the area covered by the adhered cell monolayer film on the sensor surface. Imaging and analyzing the sensors after the QCM-D experiments (Figures 3-D, S1D-F and S-2) , we found that with an increase in the $H_2O_2$ concentration, there was an increase in the number of

dead cells which contributes to increasing surface rigidity-decreasing Δ*D*-response curves[52]. Notably, cell detachment may have taken place as an event of apoptosis due to oxidative stress[52]. Even though we did not directly observe the process of cell monolayer desorption, microscopy images (Figure S-2) showing empty spaces on the sensor surface indicate the removal of mass from the sensor surface which would contribute to the QCM-D signals. Considering the fact that with increasing $H_2O_2$ concentration, there is an increase in the number of dead cells, one might expect the decline of Δ*D*-response curve for 25 μM $H_2O_2$ when compared to the control. However, such is the case if one were to only relate the stiffness of the dead cells with the Δ*D*-response. Imaging results demonstrated that for 25 μM $H_2O_2$, cells were still confluent and well spread on the sensor surface, appearing similar to the control. Interestingly, with 25 μM $H_2O_2$, the average nucleus size appeared to be slightly increased as opposed to the results of higher concentration treatment. Even though very few cells appeared apoptotic, they were still attached to the sensor surface and contributed to the Δ*D*-response curve. Past studies have also shown that factors such as modification and strength of adhesion proteins, production of various proteins within the cells, density and type of binding proteins, etc., influence the Δ*D*-response generated by cell monolayer[53], [54]. This could mean that in this study, the production of antioxidant proteins might have contributed to the Δ*D*-response via multiple dissipative processes. The aforementioned results indicate that Δ*D*-response was influenced by various factors arising from the oxidative stress-induced biochemical and physical events which have gray zones between the associated processes and are more likely to occur in a concerted manner rather than sequential.

In this study, the occurrence of oxidative biochemical events triggering the production of antioxidants has been confirmed by the TAC assay which mainly demonstrated that when cells

were treated with 25 μM $H_2O_2$, the TAC recovered at the recovery point which agrees well with our QCM-D results at the recovery point (t=325min). The return of the 25 μM $H_2O_2$ Δ*D*-response curve close to the baseline and intersection with the control Δ*D*-response may suggest that MC3T3 cells may have been subjected to oxidative eustress. According to scientific literature, oxidative eustress occurs when cells are exposed to low concentrations of ROS. Signaling pathways involving the Nrf2/Keap1 system are activated which stimulate the antioxidant response element in the nucleus leading to the production of antioxidant defense systems[6], [8], [9], [17]. This mechanism produces enough antioxidants to adequately quench excess amounts of ROS. Hence, cells regain balance in their redox state and enter back into the normal cell cycle performing their general functions with minimal or no change in cell morphology[7], [18]. With higher $H_2O_2$ concentration treatment (50 μM-10 mM), we observed decline in the Δ*D*-response curves. We speculate that oxidative distress may have occurred in cells treated with $H_2O_2$ > 25 μM. According to previous reports, oxidative distress occurs due to the exposure of cells to high ROS concentrations, during which complex signaling pathways involving NF- κB, JNK, AP-1, p53 and MAP kinases are activated. These systems not only up-regulate the generation of antioxidant enzymes but also activate expression of inflammation proteins and trigger the onset of cell-senescence, apoptotic/necrotic pathways which lead to recoding of cellular function[55]. Additionally, oxidative distress causes the impairment of the cellular antioxidant defense mechanisms depending on the ROS concentration[3], [4], [7]–[9]**.** At high intensity of oxidative stress, the fate of cells is mostly necrosis[6], [8], [18]. This could explain the non-recovery and the constant decline in the Δ*D*-responses due to $H_2O_2$ concentrations > 25 μM which could be associated with progressive cell death due to oxidative damage. Evidenced by the TAC results, increasing $H_2O_2$ concentration treatment led to the

decline of TAC levels in cells which could be due to the destruction of important cellular components and the onset of signals associated with oxidative distress[6], [8], [9].

Considering the $H_2O_2$ concentration-dependent rate of cytotoxicity[56], [57] and our results from the TAC assay, we speculate that the peak in the Δ*D*-response is influenced primarily by the activity of the antioxidant defense mechanisms in cells and the associated cell physiological changes which directly affects the viscoelastic properties of the adherent cell monolayer. We speculate so because the highest peak was observed with 50 μM $H_2O_2$ Δ*D*-response shortly after the removal of $H_2O_2$, which coincided with the TAC assay results where the highest concentrations of antioxidants were detected in cells after the removal of 50 μM $H_2O_2$. On the other hand, for $H_2O_2$ > 50 μM, the peaks appeared before the removal of $H_2O_2$. The peak may indicate a point beyond which the cells cannot cope up with the chemical stress induced. This means even after the removal of 50 μM $H_2O_2$, the antioxidant defense system was serving to counterbalance the effects of 50 μM $H_2O_2$ until the point represented by the peak. But the accumulative oxidative damage may have overtaken the antioxidant system increasing sensor surface rigidity and hence, led to the decline in the Δ*D*-response. 10 mM $H_2O_2$, being the highest concentration tested, generated the initial peak faster than the other concentrations tested. As expected, the cell membrane was already ruptured in the necrotic cells fixed after the removal of 10 mM $H_2O_2$ (Figure 5-A), which may have caused the leakage of intracellular contents and thus, loss of antioxidants. This explains the non-detectable levels of antioxidants in 10 mM $H_2O_2$ treated cells (Figure 6). The events of apoptosis, necrosis and cytoskeleton retraction as a result of high concentrations of $H_2O_2$ were confirmed by fluorescence imaging (Figure 4-A). The results demonstrated that with $H_2O_2$ concentration > 25 μM, there was an increase in the cell cytoskeleton shrinkage and also, visible progressive stages of apoptosis via chromatin condensation, and nuclear

fragmentation[22], [30], [58]–[62]. These observations agree with previous studies outlining cell death and reorganization of actin cytoskeletal structure as a function of the concentration of the oxidative agent [22], [30], [58]–[62]. Furthermore, reduction in cell viability (Figure 3-D and Figure S-2) observed with increasing concentration, likely related with the reduction in live/dead ratio for cells attached to sensors post QCM-D experiments (Figure S1-E).

However, events occurring during oxidative distress tend to be complicated because cells may demonstrate a combined event of both adaptive and damaging response. Some may have permanently damaged molecules and cellular components, while others may show early stages of apoptosis. This is because the events of apoptosis and necrosis in the cell population can be unsynchronized which is due to the highly variable duration of the initiation phase of cell death[57], [63], [64]. This means some cells treated with the same high concentration may exhibit slow and delayed oxidative damage leading to delayed and varying cell death and detachment rates. Very few cells may enter back into the cell cycle with altered function and morphology, hence, disturbing the homeostasis[6]–[8]. This explains the appearance of second peak for 100 μM $\Delta D$-response curve which may be associated with delayed cytotoxic response in some cells. Moreover, the plateau in the 10 mM $\Delta D$-response curve around the recovery point may be caused by the overall delayed and slow cytotoxic response in the very few still attached to the sensor surface. The varying and unsynchronized cellular response to the same $H_2O_2$ concentration has been confirmed by the distinct altered morphology of MC3T3 cells in the same sample of fixed cells (Figure 5). This variation resulted in the uneven spatial distribution of cells on the sensor surface (Figure 5 and Figure S-4). While recovery in cell morphology was obtained after cell treatment with low (25 μM $H_2O_2$) concentration, higher concentrations resulted in altered cell morphology characteristic of oxidative stress, eventually leading to cell lysis and cell death[13],

[14], [58], [60], [65]. Therefore, it is evident that SEM and AFM results on morphological changes of MC3T3 cells due to oxidative stress correlate well with the Δ*D*-response curves from our QCM-D measurements.

In this study, we have also shown that the Δ*D*-response is a far more sensitive and direct measure of the changes in the complex set of viscoelastic properties induced by $H_2O_2$ than the Δ*f*-response. Even though distinct Δ*f*-responses were detected for each $H_2O_2$ concentration tested, the imaging and biochemical assay results could not be related to the Δ*f*-response curves (Figure S1-C). Such low detection sensitivity is probably reflective of the fact that Δ*f*-response mostly measures the changes associated with the protein composition of the cell adhesion complex which is limited to the mass change in a localized and confined basal area of the cell monolayer[66], [67]. Additionally, we speculate that PDL-coating utilized to facilitate cellular attachment to the sensor surface may have interfered with the detection sensitivity of the Δ*f*-response. At this stage, we can only speculate these results, also supported by previous studies. For example, strong shifts in Δ*D*-response curves were demonstrated as a result of adhesion of small fraction of the cell membrane, whereas the contact of the cells with the substrate induced only a small decrease of Δ*f*-response which was not proportional to the actual mass adsorbed to the sensor surface[67].For the control group, we observed decrease in the Δ*f*-response for the entire experiment. It is possible that this decline is majorly influenced by the maturation of the focal adhesion complexes (Figure S1-C)[67]. Interestingly, for the control group, we observe an initial increase in the Δ*D*-response curve (Figure 3-C). This could be related to the minor cytoskeletal rearrangements and other changes in the protein adhesion complexes under flowing conditions. After about an hour into the experiment, Δ*D*-response demonstrated a gradual decrease (Figure 3-C), which confirms that cells entered attained a steady state where further maturation of the adhesion proteins and production of

extracellular matrix may have resulted in the decrease of both Δ*f*- and Δ*D*-response curves. These observations further confirm that even though $H_2O_2$-induced changes in the cell interaction could influence the Δ*f*-response, majority of the information on cellular state is provided by the energy dissipation factor. Such high sensitivity of the Δ*D*-response is probably related to the high level of energy dissipation contributed collectively from the concerted series of events taking place in cells as a result of oxidative stress.

Overall, the results from the complementary studies correlated with each $H_2O_2$-induced Δ*D*-response and suggested that changes in various factors influenced the viscoelastic properties of cells including changes in the cell cytoskeletal structure, cell viability and density, cell morphology and surface area coverage, biochemical events during oxidative stress and the associated physiological state of cells. These factors collectively influence the stiffness of the cell monolayer which affects the overall rigidity of the sensor surface- higher the $H_2O_2$ concentration (> 25 μM), greater the sensor surface rigidity leading to greater decline in the Δ*D*-response curves.

## 5. CONCLUSION

In this work, a QCM-D technique was used to successfully study the effects of oxidative stress on the viscoelastic properties of a confluent cell monolayer of murine pre-osteoblast MC3T3 cells. Varying concentrations of $H_2O_2$ modulated the oxidative stress-induced response and thereby their viscoelastic properties. Real-time monitoring of cells' morphological changes induced by $H_2O_2$ using QCM-D platform provided us with corresponding Δ*D*-response fingerprints for each $H_2O_2$ concentration treatment. By obtaining cellular redox and morphological recovery with 25 μM $H_2O_2$ treatment, we could confirm that based on the Δ*D*-response behavior, the viscoelastic properties of cells can be used to investigate cell recovery from oxidative stress,

which may allow us to distinguish between oxidative eustress and distress. However, further validation is required by conducting experiments to confirm the occurrence of oxidative eustress and distress. The QCM-D data strongly correlated with the complementary cell imaging analyses, cell viability and the total antioxidant capacity assay. As such, QCM-D can be used as viable technique to monitor and detect the effects of oxidative stress on cells' viscoelastic properties associated with the morphological changes.

Our future work includes studying the effect of varying $H_2O_2$ concentrations on other types of cells with varying incubation period. Considering the high sensitivity of the $\Delta D$-response demonstrated in this study, we expect similar but distinct results for each experimental condition. Moreover, it will be worthwhile to combine fluorescence imaging with QCM-D studies to better investigate the relationship between the $H_2O_2$-induced real-time changes in the focal adhesion proteins, rate of cell detachment, and the associated $\Delta D$-response curves. This may also allow us to get a clearer insight into the $\Delta f$-response. Additionally, we will be able to quantify the surface area covered by the cell monolayer on each sensor surface, specifically area covered by the live and dead cells. By employing these future experimental approaches and by conducting further studies we want to attain a further mechanistic and quantitative understanding of the correlation between the $H_2O_2$-induced viscoelastic changes in the adhered cell monolayer and the associated changes in the energy dissipation. In the far future, this direction will allow us to design and develop an *in vitro* model to investigate bone disease associated with oxidative stress.

## 6. ASSOCIATED CONTENT

Supplementary results involving, $\Delta f$-response profile, QCM-D control experiment and live/dead ratio analysis, light microscopy images of cell monolayer attached to sensors post QCM-D experiment, AFM results showing the effect on the lateral distance of MC3T3 cells due

to oxidative stress, SEM image analysis – bar graph showing the percentage surface area covered by the cell monolayer, and tabulated version of statistical analysis on TAC results.

## 7. AUTHOR INFORMATION


### Corresponding Author

*Email: maryam.tabrizian@mcgill.ca

*Address: 3775, University Street, Montreal, QC, Canada, H3A 2B4


### Author Contributions

The manuscript was written through contributions of all authors

Note: The authors declare no competing financial interest and no conflict of interest.

## 9. REFERENCES


[1] H. Sies, "Oxidative stress: A concept in redox biology and medicine," *Redox Biol.*, vol. 4, pp. 180–183, 2015.

[2] M. Breitenbach and P. Eckl, "Introduction to oxidative stress in biomedical and biological research," *Biomolecules*, vol. 5, no. 2, pp. 1169–1177, 2015.

[3] A. Rahal *et al.*, "Oxidative stress, prooxidants, and antioxidants: The interplay," *Biomed Res. Int.*, vol. 2014, 2014.

[4] A. Görlach *et al.*, "Reactive oxygen species, nutrition, hypoxia and diseases: Problems solved?," *Redox Biol.*, vol. 6, pp. 372–385, 2015.

[5] G. Pizzino *et al.*, "Oxidative Stress: Harms and Benefits for Human Health," *Oxid. Med. Cell. Longev.*, vol. 2017, 2017.

[6] V. I. Lushchak, "Free radicals, reactive oxygen species, oxidative stress and its classification," *Chem. Biol. Interact.*, vol. 224, pp. 164–175, 2014.

[7] M. Schieber and N. S. Chandel, "ROS function in redox signaling and oxidative stress,"

*Curr. Biol.*, vol. 24, no. 10, pp. R453–R462, 2014.

[8] V. I. Lushchak, "Adaptive response to oxidative stress: Bacteria, fungi, plants and animals," *Comp. Biochem. Physiol. - C Toxicol. Pharmacol.*, vol. 153, no. 2, pp. 175–190, 2011.

[9] E. Niki, "Oxidative stress and antioxidants: Distress or eustress?," *Arch. Biochem. Biophys.*, vol. 595, pp. 19–24, 2016.

[10] H. Sies, "Hydrogen peroxide as a central redox signaling molecule in physiological oxidative stress: Oxidative eustress," *Redox Biol.*, vol. 11, no. December 2016, pp. 613–619, 2017.

[11] H. Cui, Y. Kong, and H. Zhang, "Oxidative Stress, Mitochondrial Dysfunction, and Aging," *J. Signal Transduct.*, vol. 2012, pp. 1–13, 2012.

[12] E. Ho, K. Karimi Galougahi, C. C. Liu, R. Bhindi, and G. A. Figtree, "Biological markers of oxidative stress: Applications to cardiovascular research and practice," *Redox Biol.*, vol. 1, no. 1, pp. 483–491, 2013.

[13] V. Houot, P. Etienne, A. S. Petitot, S. Barbier, J. P. Blein, and L. Suty, "Hydrogen peroxide induces programmed cell death features in cultured tobacco BY-2 cells, in a dose-dependent manner," *J. Exp. Bot.*, vol. 52, no. 361, pp. 1721–1730, 2001.

[14] L. Xu *et al.*, "Hydrogen peroxide induces oxidative stress and the mitochondrial pathway of apoptosis in RAT intestinal epithelial cells (IEC-6)," *Mol. Biol.*, vol. 50, no. 2, pp. 270–277, 2016.

[15] T. Kiyoshima *et al.*, "Oxidative stress caused by a low concentration of hydrogen peroxide induces senescence-like changes in mouse gingival fibroblasts," *Int. J. Mol. Med.*, vol. 30, no. 5, pp. 1007–1012, 2012.

[16] A. A. Fatokun, T. W. Stone, and R. A. Smith, “Hydrogen peroxide-induced oxidative stress in MC3T3-E1 cells: The effects of glutamate and protection by purines,” *Bone*, vol. 39, no. 3, pp. 542–551, 2006.

[17] H. S. Marinho, C. Real, L. Cyrne, H. Soares, and F. Antunes, “Hydrogen peroxide sensing, signaling and regulation of transcription factors,” *Redox Biol.*, vol. 2, no. 1, pp. 535–562, 2014.

[18] S. García-Santamarina, S. Boronat, and E. Hidalgo, “Reversible cysteine oxidation in hydrogen peroxide sensing and signal transduction,” *Biochemistry*, vol. 53, no. 16, pp. 2560–2580, 2014.

[19] N. Mody, F. Parhami, T. A. Sarafian, and L. L. Demer, “Oxidative stress modulates osteoblastic differentiation of vascular and bone cells,” *Free Radic. Biol. Med.*, vol. 31, no. 4, pp. 509–519, 2001.

[20] G. J. Burton and E. Jauniaux, “Oxidative stress,” *Best Pract. Res. Clin. Obstet. Gynaecol.*, vol. 25, no. 3, pp. 287–299, 2011.

[21] D. Trachootham, W. Lu, M. A. Ogasawara, N. R. Valle, and P. Huang, “Comprehensive Invited Review,” *Antioxid. Redox Signal.*, vol. 10, no. 8, pp. 1344–1365, 2008.

[22] D. Zhu, “Hydrogen peroxide alters membrane and cytoskeleton properties and increases intercellular connections in astrocytes,” *J. Cell Sci.*, vol. 118, no. 16, pp. 3695–3703, 2005.

[23] M. A. M. Ali, A. D. Kandasamy, X. Fan, and R. Schulz, “Hydrogen peroxide-induced necrotic cell death in cardiomyocytes is independent of matrix metalloproteinase-2,” *Toxicol. Vitr.*, vol. 27, no. 6, pp. 1686–1692, 2013.

[24] X. C. Bai *et al.*, “Oxidative stress inhibits osteoblastic differentiation of bone cells by

ERK and NF-κB," *Biochem. Biophys. Res. Commun.*, vol. 314, no. 1, pp. 197–207, 2004.

[25] H. Cui, Y. Kong, and H. Zhang, "Oxidative Stress, Mitochondrial Dysfunction, and Aging," *J. Signal Transduct.*, vol. 2012, pp. 1–13, 2012.

[26] N. Tymchenko, E. Nileba, M. V. Voinova, J. Gold, B. Kasemo, and S. Svedhem, "Reversible changes in cell morphology due to cytoskeletal rearrangements measured in real-time by QCM-D," *Biointerphases*, vol. 7, no. 1–4, pp. 1–9, 2012.

[27] E. Moeendarbary and A. R. Harris, "Cell mechanics: Principles, practices, and prospects," *Wiley Interdiscip. Rev. Syst. Biol. Med.*, vol. 6, no. 5, pp. 371–388, 2014.

[28] I. Basu *et al.*, "Morphological and cytoskeletal changes caused by non-membrane damaging cytotoxin of Vibrio cholerae on Int 407 and HeLa cells," *FEMS Microbiol. Lett.*, vol. 179, no. 2, pp. 255–263, 1999.

[29] M. A. Wozniak, K. Modzelewska, L. Kwong, and P. J. Keely, "Focal adhesion regulation of cell behavior," *Biochim. Biophys. Acta - Mol. Cell Res.*, vol. 1692, no. 2–3, pp. 103–119, 2004.

[30] I. Dalle-Donne, R. Rossi, A. Milzani, P. Di Simplicio, and R. Colombo, "The actin cytoskeleton response to oxidants: From small heat shock protein phosphorylation to changes in the redox state of actin itself," *Free Radic. Biol. Med.*, vol. 31, no. 12, pp. 1624–1632, 2001.

[31] D. A. Fletcher and R. D. Mullins, "NIH Public Access," vol. 463, no. 7280, pp. 485–492, 2010.

[32] D. A. Fletcher and R. D. Mullins, "Cell mechanics and the cytoskeleton," vol. 463, no. January, pp. 485–492, 2010.

[33] I. Marrocco, F. Altieri, and I. Peluso, "Measurement and Clinical Significance of

Biomarkers of Oxidative Stress in Humans," *Oxid. Med. Cell. Longev.*, vol. 2017, 2017.

[34] G. I. Zahalak, W. B. McConnaughey, and E. L. Elson, "Determination of Cellular Mechanical Properties by Cell Poking, With an Application to Leukocytes," *J. Biomech. Eng.*, vol. 112, no. 3, p. 283, 1990.

[35] R. M. Hochmuth, "Micropipette aspiration of living cells," *J. Biomech.*, vol. 33, no. 1, pp. 15–22, 2000.

[36] K. A. Addae-Mensah and J. P. Wikswo, "Measurement techniques for cellular biomechanics in vitro.," *Exp. Biol. Med. (Maywood).*, vol. 233, no. 7, pp. 792–809, 2008.

[37] M. Rodahl and B. Kasemo, "A simple setup to simultaneously measure the resonant frequency and the absolute dissipation factor of a quartz crystal microbalance," *Rev. Sci. Instrum.*, vol. 67, no. 9, pp. 3238–3241, 1996.

[38] C. Fredriksson, S. Kihlman, M. Rodahl, and B. Kasemo, "The Piezoelectric Quartz Crystal Mass and Dissipation Sensor: A Means of Studying Cell Adhesion," *Langmuir*, vol. 14, no. 2, pp. 248–251, 1998.

[39] C. Fredriksson, S. Khilman, B. Kasemo, and D. M. Steel, "In vitro real-time characterization of cell attachment and spreading," *J. Mater. Sci. Mater. Med.*, vol. 9, no. 12, pp. 785–788, 1998.

[40] M. S. Lord *et al.*, "Monitoring cell adhesion on tantalum and oxidised polystyrene using a quartz crystal microbalance with dissipation," *Biomaterials*, vol. 27, no. 26, pp. 4529–4537, 2006.

[41] C. Modin *et al.*, "QCM-D studies of attachment and differential spreading of pre-osteoblastic cells on Ta and Cr surfaces," *Biomaterials*, vol. 27, no. 8, pp. 1346–1354, 2006.

[42] D. Wang, C. Kurt, K. Chawla, G. Xiao, P. H. Krebsbach, and R. T. Franceschi, “Isolation and Characterization of MC3T3-E1 Vivo Differentiation / Mineralization Potential,” *J. Bone Miner. Res.*, vol. 14, no. 6, pp. 893–903, 1999.

[43] O. C. Formation and M. Kumegawa, “Mouse Osteoblastic Cells ( MC3T3-E1 ) at Different,” vol. 128, no. 3, pp. 1630–1637, 2015.

[44] V. Domazetovic, “Oxidative stress in bone remodeling: role of antioxidants,” *Clin. Cases Miner. Bone Metab.*, vol. 14, no. 2, p. 209, 2017.

[45] J. Y. Chen, A. Shahid, M. P. Garcia, L. S. Penn, and J. Xi, “Dissipation monitoring for assessing EGF-induced changes of cell adhesion,” *Biosens. Bioelectron.*, vol. 38, no. 1, pp. 375–381, 2012.

[46] P. Spaepen, S. De Boodt, J. Aerts, and J. Vander Sloten, “Mammalian Cell Viability,” vol. 740, no. March, 2011.

[47] S. R. Sripathi *et al.*, “Nitric oxide leads to cytoskeletal reorganization in retinal pigment epithelium under oxidative stress,” *Adv Biosci Biotechnol*, vol. 8, no. 5, pp. 583–592, 2012.

[48] D. P. D’Agostino, J. E. Olson, and J. B. Dean, “Acute hyperoxia increases lipid peroxidation and induces plasma membrane blebbing in human U87 glioblastoma cells,” *Neuroscience*, vol. 159, no. 3, pp. 1011–1022, 2009.

[49] J. Xi and J. Y. Chen, “Quartz Crystal Microbalance in Cell Biology Studies,” *J. Biochips Tissue Chips*, vol. s5, pp. 1–9, 2013.

[50] J. Fatisson, F. Azari, and N. Tufenkji, “Real-time QCM-D monitoring of cellular responses to different cytomorphic agents,” *Biosens. Bioelectron.*, vol. 26, no. 7, pp. 3207–3212, 2011.

[51] K. M. Schmoller, O. Lieleg, and A. R. Bausch, “Structural and viscoelastic properties of actin/filamin networks: Cross-linked versus bundled networks,” *Biophys. J.*, vol. 97, no. 1, pp. 83–89, 2009.

[52] N. I. Nikolaev, T. Müller, D. J. Williams, and Y. Liu, “Changes in the stiffness of human mesenchymal stem cells with the progress of cell death as measured by atomic force microscopy $$,” *J. Biomech.*, vol. 47, no. 3, pp. 625–630, 2014.

[53] C. Fredriksson, S. Kihlman, M. Rodahl, and B. Kasemo, “The Piezoelectric Quartz Crystal Mass and Dissipation Sensor: A Means of Studying Cell Adhesion,” *Langmuir*, vol. 14, no. 2, pp. 248–251, 1998.

[54] N. Tymchenko *et al.*, “Reversible Changes in Cell Morphology due to Cytoskeletal Rearrangements Measured in Real-Time by QCM-D Reversible Changes in Cell Morphology due to Cytoskeletal Rearrangements Measured in Real-Time by QCM-D,” vol. 43, pp. 1–10, 2012.

[55] M. Li *et al.*, “Hydrogen peroxide induces G2cell cycle arrest and inhibits cell proliferation in osteoblasts,” *Anat. Rec.*, vol. 292, no. 8, pp. 1107–1113, 2009.

[56] M. Gülden, A. Jess, J. Kammann, E. Maser, and H. Seibert, “Free Radical Biology & Medicine Cytotoxic potency of H 2 O 2 in cell cultures : Impact of cell concentration and exposure time,” *Free Radic. Biol. Med.*, vol. 49, no. 8, pp. 1298–1305, 2010.

[57] M. Li *et al.*, “Hydrogen Peroxide Induces G 2 Cell Cycle Arrest and Inhibits Cell Proliferation in Osteoblasts,” vol. 1113, no. February, pp. 1107–1113, 2009.

[58] P. Storz, H. Döppler, C. Ferran, S. T. Grey, and A. Toker, “Functional dichotomy of A20 in apoptotic and necrotic cell death,” *Biochem. J.*, vol. 387, no. 1, pp. 47–55, 2005.

[59] J. H. Song, Z. L. Ma, X. W. Chi, Y. P. Chen, and L. Hou, “The endogenous oxindole

isatin induces apoptosis of MCF-7 breast cancer cells through a p53-mediated mitochondrial pathway," *Chinese Pharmacol. Bull.*, vol. 32, no. 6, pp. 773–778, 2016.

[60] Y. qin Jin, J. ling Li, J. dong Chen, C. liang Xu, and H. Li, "Dalbergioidin (DAL) protects MC3T3-E1 osteoblastic cells against H2O2-induced cell damage through activation of the PI3K/AKT/SMAD1 pathway," *Naunyn. Schmiedebergs. Arch. Pharmacol.*, vol. 390, no. 7, pp. 711–720, 2017.

[61] P. Dai *et al.*, "Attenuation of Oxidative Stress-Induced Osteoblast Apoptosis by Curcumin is Associated with Preservation of Mitochondrial Functions and Increased Akt-GSK3β Signaling," *Cell. Physiol. Biochem.*, vol. 41, no. 2, pp. 661–677, 2017.

[62] A. Rutkovskiy, K.-O. Stensløkken, and I. J. Vaage, "Osteoblast Differentiation at a Glance," *Med. Sci. Monit. Basic Res.*, vol. 22, pp. 95–106, 2016.

[63] K. Kannan and S. K. Jain, "Oxidative stress and apoptosis," vol. 7, no. 27, pp. 153–163, 2000.

[64] E. Brauchle, S. Thude, S. Y. Brucker, and K. Schenke-layland, "Cell death stages in single apoptotic and necrotic cells monitored by Raman microspectroscopy," pp. 1–9, 2014.

[65] J. A. Hessler *et al.*, "Atomic force microscopy study of early morphological changes during apoptosis," *Langmuir*, vol. 21, no. 20, pp. 9280–9286, 2005.

[66] J. Y. Chen, A. Shahid, M. P. Garcia, L. S. Penn, and J. Xi, "Biosensors and Bioelectronics Dissipation monitoring for assessing EGF-induced changes of cell adhesion," *Biosens. Bioelectron.*, vol. 38, no. 1, pp. 375–381, 2012.

[67] C. Tonda-turo, I. Carmagnola, and G. Ciardelli, "Quartz Crystal Microbalance With Dissipation Monitoring : A Powerful Method to Predict the in vivo Behavior of Bioengineered Surfaces," vol. 6, no. October, pp. 1–7, 2018.

## Graphical Abstract